Analysis of the Effect of Soft Soil's Parameters Change on Planetary Vehicles' Dynamic Response

Submitted: 25th September 2017; accepted: 16th January 2018

Hassan Shibly

DOI: 10.14313/JAMRIS_4-2017/37

Abstract:
The mobility of a planetary vehicle has numerous constraints imposed by the types of terrain. Navigation is difficult through uneven and rocky terrain, and becomes worse due to abrupt changes of ground level which may cause a fall to a lower ground level. This article examines the effect of the soil's parameters change due to repetitive falls on the vehicle's dynamic behavior. After each free fall of the vehicle there is a collision of the vehicle's wheel with the ground. If the ground is made up of soft soil there is an increase in the soil compactness after each collision. The increase in the soil compactness causes a change in the soil parameters. These changes modify the algorithm's parameters of the vehicle's dynamic model. The dynamic model is a quarter vehicle model with single rigid wheel which falls on soft soil. Simplified forms of the Pressure-Sinkage models of Bekker and Reece for the sinkage of a rigid body into soft soil are incorporated in the numerical solution of the governing equations of motion. The dynamic interaction of a rigid wheel and soft soil has three stages: sinkage stage, wheel dwell stage, and wheel pullout from soil stage. By comparing the simulations results when the soil's parameters are kept constant and when their changes are incorporated in the dynamic model showed that the difference in the dynamic response are not significant and can be neglected. There is a gradual change in the dynamic mechanical quantities when the soil's parameters are kept constant, while the changes in the dynamic mechanical quantities between the second fall and the successive falls are small.

Keywords: *rigid wheel-soil sinkage, dynamic response of rover, sinkage by free fall, soft soil parameters change, work of normal force.*

1. Introduction

Expanding the planetary mission exploration area requires increasing the planetary vehicle's speed. Planetary mission planners carefully select the rout of planetary vehicles on the surface of a plant, although, the vehicles are expected to face an extremely complicated and challenging terrains. A motion at high speed could face an abrupt change of ground level which may lead the vehicle to fall on to a lower soft ground level. As a result; planetary vehicle's design requires a new design that enhances the navigation capability of vehicles to navigate on a various types of terrain and to be able to recover from unexpected falls. The study and simulation of the dynamic response of the vehicle for a specific type of terrain provides the designers with adequate information to adjust their design to overcome such cases.

The dynamic response of planetary vehicles after a fall on soft soil has not been investigated enough. Such a situation is expected in any planetary exploration mission, as well as off road vehicles. The special thing of such a case is the dynamic interaction between a rigid wheel and soft soil during the penetration of the wheel until its maximum sinkage. This study and simulation examining the dynamic response of a planetary vehicle (rover) during multiple falls on soft soil which are initiated by an abrupt change of the ground level. The analysis of falling on soft soil which leads to the sinkage of the rover's rigid wheel into the soft soil requires the use of Pressure-Sinkage relations.

Many researchers investigated the pressure sinkage relationship of the sinkage of a rigid body that penetrates into soft soil by applying a normal load. The majority of them used rigid flat plates as a rigid body. Experiments were performed by loading the plate and measuring force and sinkage into the soil assuming homogeneous terrain in the vertical direction of the sinkage, it is called Bevameter technique.

One of the earlier reported model for pressure--sinkage relationship used in terra mechanics was [1], [2]. The model, Equation (1), is a fundamental empirical formula developed to estimate the pressure-sinkage relationship of a rigid body that sinks into soil under a uniform pressure.

$$p = kz^n \tag{1}$$

Where z soil sinkage, k soil deformation modulus, n constant, and p loading pressure.

In order to measure penetration interaction mechanics into soil under vertical loads loaded plates were used, Bevameter tests. For a homogeneous soil, the pressure-sinkage relationship equation (2) was proposed by [3], and [4]. Bekker introduced an empirical model for the pressure-sinkage relationship by replacing k with $(k_c/b + k_\varphi)$ as shown in Equation (2).

$$p = \left(\frac{k_c}{b} + k_\emptyset\right) z^n \tag{2}$$

Where p is the uniform load pressure applied on the flat plate measured at z sinkage, n is the soil material sinkage exponent experimentally obtained and de-

fines the curvature of the pressure-sinkage curve of a soil under normal load, k_c [kN/m^{n+1}] the cohesion module, k_ϕ [kN/m^{n+2}] the friction module of the soil, and b is the smallest width of the loaded flat plate. Example of soil parameters are given in Table 1. To demonstrate the effect of the soil exponent n on the pressure-sinkage curve, a five curves were plotted as shown in Figure 1 based on the empirical values of Table 1.

***Table 1. Bekker pressure-sinkage model parameters for three terrains* [5]**

Terrain Type	Content of Moisture	Soil Exponent n	Cohesion Module k_c	Friction Module k_ϕ	Cohesion c	Friction Angle ϕ[deg.]
Dry Sand	0.0%	1.10	0.99	1528.40	1.04	28.0
Lete Sand	0.0%	0.79	102.00	5301.00	1.30	31.1
Loam	46.0%	0.73	41.60	2471.00	0.691	33.3
Clay	38.0%	0.50	13.19	692.00	4.14	13.0
Heavy Clay	25.0%	0.13	12.70	1555.59	68.95	34.0

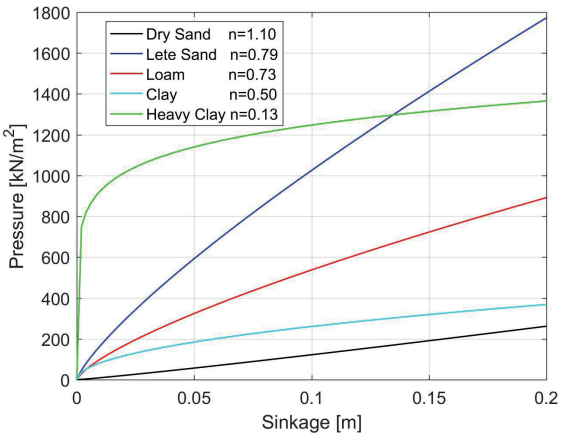

Fig. 1. Pressure-sinkage curves for sand, loam, and clay soils

Upadhyaya, et al. [6] proposed a modified form of Bekker model, Equation (2), by normalizing the sinkage of the plat width as shown in Equation (3)

$$p = (k_1 + bk_2)\left(\frac{z}{b}\right)^n \tag{3}$$

Where k_1 [kPa] and k_2 [kPa/m] are the soil sinkage constants and are independent of the plate dimension.

To obtain the soil sinkage constants a set of experiments have to be done by using two plates with different sizes [6]. In order to minimize soil variations in the test there is a need to have a large difference in the plates' sizes. The measured data sets of the pressure sinkage were analyzed theoretically and graphically to obtain the best fit using logarithmic scale. From the straight line best fit the values of the constants were obtained.

Based on experimental results Reece [7] proposed a new and non-dimensional model for the pressure-sinkage relationship as it shown in Equation (4).

$$p = \left(ck_c' + \gamma bk_\phi'\right)\left(\frac{z}{b}\right)^n \tag{4}$$

Where c soil cohesion, γ unit weight density of soil, and k_c', k_ϕ', are dimensionless constants of the cohesion and friction module, and n soil exponential constant. Wong [4] recommends that ck_c' term is negligible for cohesion less dry sand, and the term that includes k_ϕ' is negligible for frictionless terrain as clay.

The conversion between the soil's parameters in the three pressure-sinkage models are:

$$k_c' = \left(\frac{b^{n-1}}{c}\right)k_c = \left(\frac{1}{c}\right)k_1$$
$$k_\phi' = \left(\frac{b^{n-1}}{\gamma}\right)k_\phi = \left(\frac{1}{\gamma}\right)k_2 \tag{5}$$

Meirion et al. modified the pressure-sinkage models for small wheels ranging from 01–0.3 meters and increased the load up to 450 newton. The proposed model, [8], considering wheel diameter is given by Equation (6).

$$p = kz^n d^m \tag{6}$$

Where d wheel diameter and m a fitting diameter exponent constant and for dry sand $m = 0.39$ [8].

The soil pressure-sinkage relation for a repetitive loading and unloading was described by [9] as shown in Equation (7).

$$p = \left(\frac{k_c}{b} + k_\phi\right)z_A^n - k_A(z_A - z) \tag{7}$$

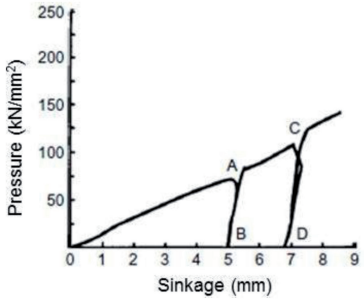

Fig. 2. Soil response to repetitive loading-unloading [9]

The line segment from zero to point A describes the first continuous loading. At point A the maximum sinkage is z_A. At point A the unloading process starts toward point B. At point B the pressure is zero while the residual sinkage is z_r. The second continuous reloading starts from point B toward point A back to the maximum sinkage z_A. From Point A toward point C the new sinkage will continue to follow the same original pressure-sinkage curve. For more loading and unloading process this curve repeats itself. During elastic reloading or unloading, line $\widehat{AB}$ on the soil response of

repetitive loading-unloading curve can be considered as the soil stiffness to loading, and experiments showed that a good approximation is that the pressure is a linear function of the total sinkage measured from the uncompact soil surface as given in Equation (8):

$$k_A = k_0 + k_{uA} z_A \tag{8}$$

The parameters k_0 $[kN/m^3]$ and k_{uA} $[kN/m^2]$ are soil specific parameters, k_A is the slope of the loading--unloading curve and depends on z_A sinkage. A graphical description for the relation between soil stiffness k_A and initial unloading sinkage is shown in Figure 3.

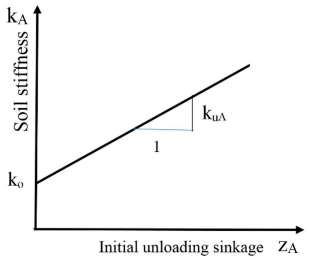

Fig. 3. Relationship between soil stiffness and initial unloading sinkage

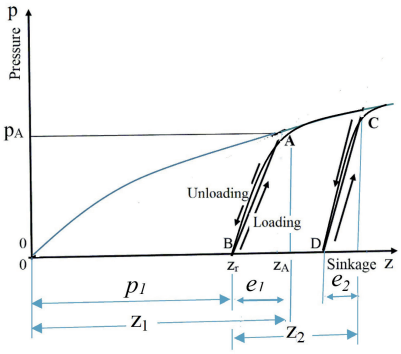

Fig. 4. Soil pressure-sinkage behavior under loading--unloading process

It can be noticed from Equation (8) that higher sinkage z_A at the end of the first loading results in more soil compaction, therefore the elastic rebound ($e_1 = z_A - z_r$) is reduced during unloading, and the elastic rebound moves the total sinkage back to z_A. A second loading of the soil starts with elastic reloading where the sinkage increases up to z_A and continues to follow the original pressure-sinkage curve $\widehat{OAC}$ for pressure larger than p_A. The first loading-unloading fall produces a plastic deformation p_1 and elastic deformation e_1 so that the first maximum sinkage $z_1 = z_A = p_1 + e_1$, and a second loading by a second fall over the same location produces an elastic deformation from point B to A which is equal to e_1. The second maximum sinkage consists of plastic and elastic deformation so that $z_2 = p_2 + e_2$ as it is described in Figure 4. It can be realized that Wong model, as it is shown in Figure 2, is not the best choice to use because of its piecewise behavior which does not follow a monotonic sinkage. Earlier works [10], [11] for finding the wheel-terrain rolling resistance for multi-pass case assumed that pressure-sinkage behavior remains the same for all passes. Experimental works of [12], [13], and [14] showed variation in the soil reaction forces under a consecutive pass by the rear wheels as a result of variations in the soil compaction and density. Therefore the terramechanics expression has to be modified to include the effect of soil compaction under repetitive loading and unloading.

Extensive experimental work was done by [14] to test the multiple wheel passages. Holm tested multiple pass of wheels on the same patch considering slip and tire deflection. The study shows that soil properties change after each pass, and the soil properties variations are strongly dependent on the wheel slip, therefore the driven wheel produces a stronger effect on soil properties variation than a towed wheel. Loading and unloading on the same soil spot of wheel multi passage case is analogical to wheel multi falls on the same soil spot. Therefore the results of the wheel multi passage are used in this analysis. Similarly, each fall of the wheel will experience new soil properties compared to the previous fall.

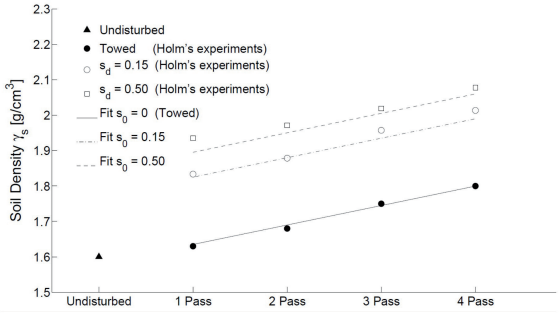

Fig. 5. Terrain properties variation for multiple passages [14], (sd: slip ratio)

Soil properties as cohesion and density increase after each passage, and the largest increase occurs between the first and second pass, while for the successive runs the increase in these properties becomes less and less. Based on Holm's experimental results as it is shown in Figure 5. Senatore and Sandu [15] came up with a number of fitted relations which relate soil properties as function of previous number of passages and slip ratio. The proposed relations for density and cohesion are shown in Equations (9–11).

$$\gamma_n = \gamma_o \left[1 + \left(1 - e^{\frac{-i_p}{k_1}} \right) k_2 + k_3 n_p \right] \tag{9}$$

$$c_n = c_o \left[1 + \left(1 - e^{\frac{-i_p}{k_1}} \right) k_2 + k_3 n_p \right] \tag{10}$$

Where; index n for value at the current passage, index *o* for value of untouched soil, n_p number of previous passages, i_p slip ratio at previous passage, γ soil density, c soil cohesion , K soil shear displacement modulus, $k1$, $k2$, and $k3$ are dimensionless fitting constants. Example of values are shown in Table 2.

Table 2. Example of soil parameters for multipass simulation [15]

n [-]	c [N/m^2]	ϕ [deg]	k_c [kN/m^{n+1}]	k_ϕ [kN/m^{n+2}]	k_1 [-]	k_2 [-]	k_3 [-]
1	220	33.1	1400	820	0.1178	0.1672	0.0348

Rewrite Equations (9–10) for the case of zero slip ratio i_p=0 to obtain a simplified form:

$$\gamma_n = \gamma_o(1 + k_3 n_p) \tag{11}$$

$$c_n = c_o(1 + k_3 n_p) \tag{12}$$

In this case the change in the two soil properties is the same and it is equal to $k_3 n_p$. The relative change in accuracy is defined by the accuracy of the fitting coefficient k_3. The relative changes in percentage for a fitting coefficient value of 0.0348 and for various number of passages are given in Table 3.

Table 3. Relative change in soil's properties

n_p Number of previous passages	1	2	3	4	5
%Relative change	3.48	6.96	10.44	13.92	17.40

Previous experimental work of pressure-sinkage on sand using three plates with different diameters was done by [16] to investigate the evolution of sand bearing capacity with density. His work results were presented graphically showing the dependency of Bekker's coefficients, k_c, k_ϕ, and n with sand density. The value of k_c determined is often negative for dry granular soil [17]. Based on his results a curve fitting is done to find an analytical dependency of the two coefficients as a function of the sand density. The fittings are given in Equations (13) and (14).

$$k_c = 54.1103\gamma^3 - 297.7516\gamma^2 + 533.0698\gamma - 312.9684 \tag{13}$$

$$k_\phi = 6.7547\gamma^3 - 20.5060\gamma^2 + 16.4391\gamma - 1.0548 \tag{14}$$

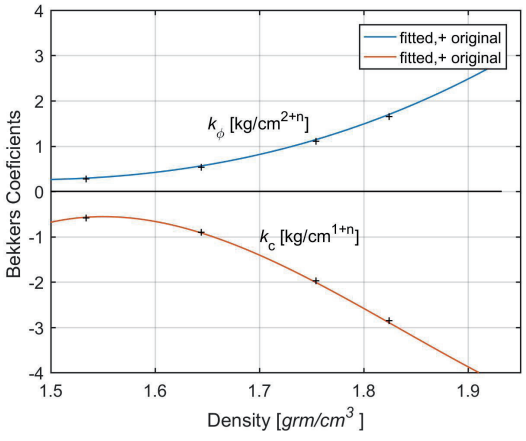

Fig. 6. Curve fitting of Bekker's coefficients dependency on soil density based on [16] experimental data

2. Rigid Wheel-Soft Soil Analysis

Previous research works by Shibly *et al.* [18], and Reece [7] showed that stress distribution around a rigid wheel during penetration into soft soil can be substituted with a very good accuracy by a triangular distribution for the two stress zones depicted in Figure 7. The linear equivalent stress distribution S_n of the normal stress p acts on the rigid wheel during sinkage is a triangle with two sides which are defined by:

$$S_{n1}(\theta) = \frac{\theta_1 - \theta}{\theta_1 - \theta_m} S_{nm} \;,\; S_{n2}(\theta) = \frac{\theta_2 + \theta}{\theta_2 + \theta_m} S_{nm} \tag{15}$$

Where the indices 1 and 2 refer to the right and left sides of the maximum stress location, the vertex of the triangle.

The equivalent distribution of the normal stresses is an isosceles triangle where the location of maximum stress is at $\theta = 0^o$ and spread equally in both sides so that the magnitudes of both angles are equal. The resultant of the normal stress acts on the rigid wheel is determined by integrating the equivalent stress distribution around the wheel contact considering the symmetry of the stress distribution ($\theta_1 = -\theta_2$) as shown in Equation (15).

$$F_z = 2rb\left(\int_0^{\theta_1} S_1(\theta) cos\theta \cdot d\theta\right) \tag{16}$$

Substitution of the stress distribution as in Equation (15) to obtain the vertical force F_z as

$$F_z = rbS_m\left(2\frac{1 - cos\theta_1}{\theta_1}\right) \tag{17}$$

The trigonometric parenthetical expression in Equation (17) as $0° \le \theta \le 45°$ can be approximated by fitting a straight line with slop of 0.98, Shibly [19]. Using this fitting and the geometry of this case to obtain the following relations:

$$1 - cos\theta_1 = \frac{z_m}{r},\; \theta_1 = f\sqrt{\frac{z_m}{r}} \tag{18}$$

where f = 1.4286

A more simplified form of the normal force is:

$$F_z = fbS_m\sqrt{rz_m} \tag{19}$$

Combining Equations (4) and (6) to obtain the normal stress:

$$S_m = \left(ck_c' + \gamma bk_\phi'\right)(2r)^m\left(\frac{z_m}{b}\right)^n \tag{20}$$

Where c soil cohesion, γ unit weight density of soil, and k_c', k_ϕ', and n dimensionless constants. It is recommended by [4] that ck_c' term is negligible for cohesion less dry sand, and the term that includes k_ϕ' is negligible for frictionless terrain as clay. After considerable simplifications the normal force can be obtained as:

$$F_z = G\left(ck_c' + \gamma bk_\phi'\right)(z_m)^{n+\frac{1}{2}} \tag{21}$$

Where the geometrical constant is:

$$G = \left(\frac{f\sqrt{r}}{b^{n-1}}\right)(2r)^m \tag{22}$$

The normal force F_z that acts on the rigid wheel resists the wheel penetration into the soil. This force is a function of the sinkage z_m and the soil exponent n. This function is highly nonlinear. For a specific wheel-soil parameters, the sinkage coefficient k_z as it is shown in Equation (23) is function of soil density and parameters variations.

$$k_z = G\left(ck_c' + \gamma bk_\phi'\right) \tag{23}$$

The coefficient k_z can be considered as the soil stiffness modulus in the vertical direction. As a result the soil resist force will have its final form as:

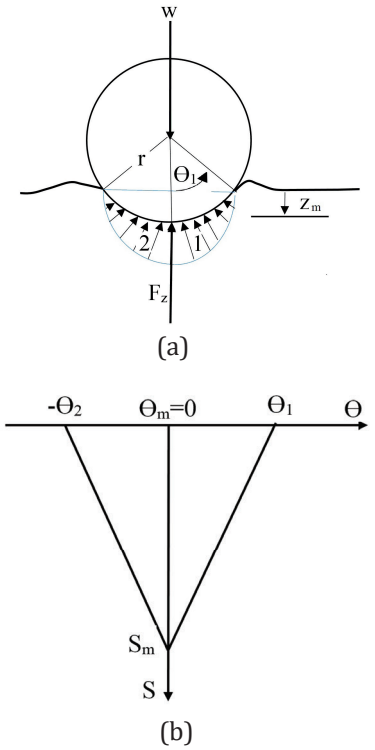

Figure 7. a) Free body diagram of rigid wheel on soft soil, b) Equivalent triangular distribution of normal stresses

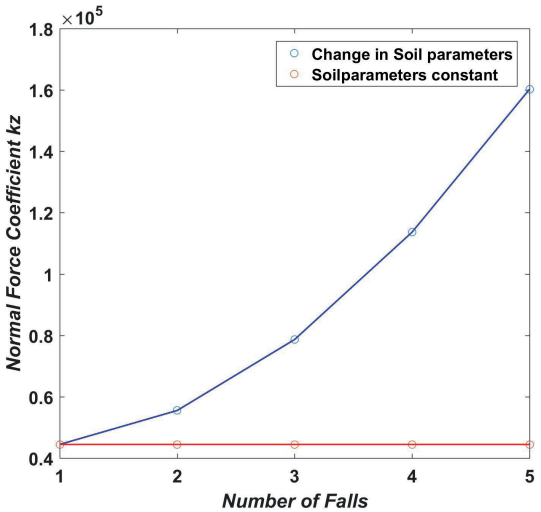

Fig. 8. The normal force coefficients at five falls for constant soil's parameters and for varying soil's parameter

$$F_z = k_z(z_m)^{n+\frac{1}{2}} \tag{24}$$

3. Dynamic Model Analysis

A four-wheel rover is composed of a platform which is connected to four wheels by a mechanical suspension. The mechanical suspension has stiffness and low damping properties. In order not to increase the nonlinearity and the complexity of the interaction with the soil a simplified linear quarter-rover model is used. The quarter rover model has two lumped masses, one quarter of the rover platform is the sprung mass m_s and the rigid wheel is the unsprung mass m_{us}. Both masses are connected by a vertical pure linear spring with high stiffness k_s and a vertical pure linear damper with a low damping coefficient c_s, a schematic drawing is shown in Figure 9.

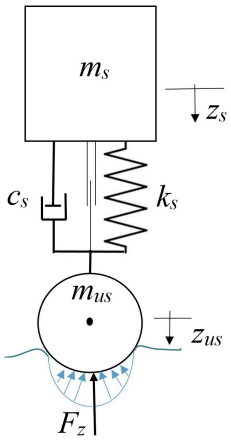

Fig. 9. Dynamic model of quarter rover

The dynamic response of the rover caused by its fall on soft soil begins by the wheel touching the soil, and the sinkage phase of the wheel starts until it reaches its maximum sinkage. The wheel remains at maximum sinkage and at rest state until it is pulled by the sprung mass if it has enough energy, and this is the dwell phase. The pulling out of the wheel from the soil is when the wheel leaves the ground to a certain height, this is the pull out phase. A second fall starts when the sprung mass reaches its zero velocity and moves down towards the soil for a second touch on the same spot of the soil.

Using newton's second law to obtain the dynamic equation of motion of a quarter rover Equations (25) and (26). The initial condition of the motion is at the instant of first soil contact has zero initial positions and initial velocity equal to the final velocities of the fall.

$$m_s\ddot{z}_s + c_s(\dot{z}_s - \dot{z}_{us}) + k_s(z_s - z_{us}) = m_s g \tag{25}$$

$$m_{us}\ddot{z}_{us} + c_s(\dot{z}_{us} - \dot{z}_s) + k_s(z_{us} - z_s) = m_{us}g - F_z \tag{26}$$

The state space representation of the dynamic equations is given in equation (27).

$$\dot{x}_1 = x_3$$

$$\dot{x}_2 = x_4$$

$$\dot{x}_3 = -\frac{k_s}{m_s}x_1 + \frac{k_s}{m_s}x_2 - \frac{c_s}{m_s}x_3 + \frac{c_s}{m_s}x_4 + g$$

$$\dot{x}_4 = \frac{k_s}{m_{us}}x_1 - \frac{k_s}{m_{us}}x_2 - \frac{k_z}{m_{us}}x_2^{\left(n+\frac{1}{2}\right)} + \frac{c_s}{m_{us}}x_3 - \frac{c_s}{m_{us}}x_4 + g \quad (27)$$

Or in a generic state space representation:

$$\dot{X} = f(X, U)$$

$$Y = h(X, U) \quad (28)$$

Where:

$$X = [x_1 \ x_2 \ x_3 \ x_4]^T \quad U = [0 \ 0 \ g \ g]^T \quad (29)$$

4. Soil Parameters Modification

The repetitive fall and pull out of the wheel increases the compactness of the soil and changes the soil's parameters. The number of falls, on the same spot, is used to calculate the new values of the soil weight density γ_n and cohesion c_n. The new soil parameters are calculated using Equations (11–14). The relations given in Equation (30) are used to obtain the dimensionless soil sinkage coefficients. Then k_z is determined based on the new soil parameters values, while Wong model for a repetitive passage is incorporated in the computer program of simulation.

$$k'_{cn} = \left(\frac{b^{n-1}}{c_n}\right) u_c k_{cn}, \ k'_{\phi n} = \left(\frac{b^{n-1}}{\gamma_n}\right) u_\phi k_{\phi n} \quad (30)$$

Where the unit conversion factors are:

$$u_c = g * (10)^{2(1+n)}, u_\phi = g * (10)^{2(2+n)} \quad (31)$$

The equations of motion are solved numerically and the simulation results are shown for: displacement-time, Figures 10 & 11, normal force-time, Figures 12 & 13, and normal force-sinkage, Figures 14 & 15. Figures 10 & 11 depict the displacement of the rover body and wheel at successive falls for a particular set of soil and dynamic model parameters. The displacement of the sprung mass in the dynamic model is plotted twice on the same figure, one plot is by itself and a second plot is shifted to be on the unsprung

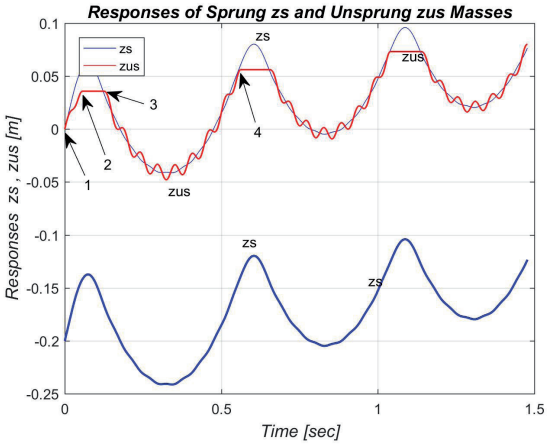

Fig. 10. The displacements of the sprung mass z_s and the wheel z_{us} during time for constant soil parameters

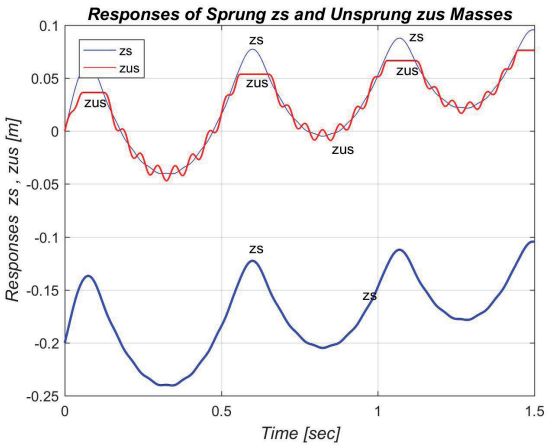

Fig. 11. The displacements of the sprung mass z_s and the wheel z_{us} during time considering soil parameters' change

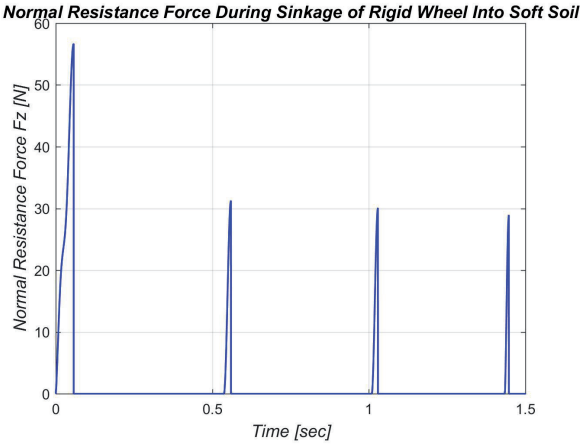

Fig. 12. The normal force which acts on the wheel during sinkage for constant soil parameters

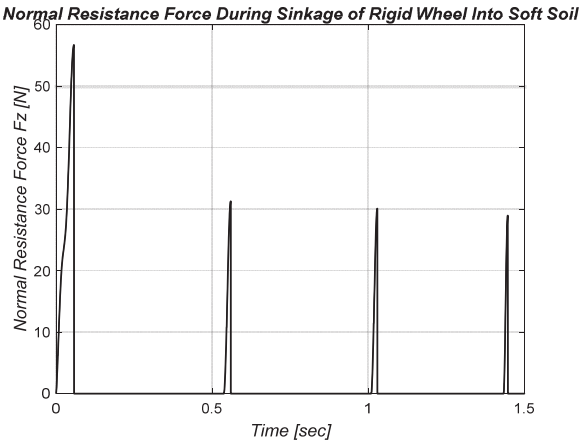

Fig. 13. The normal force which acts on the wheel during sinkage considering soil parameters' change

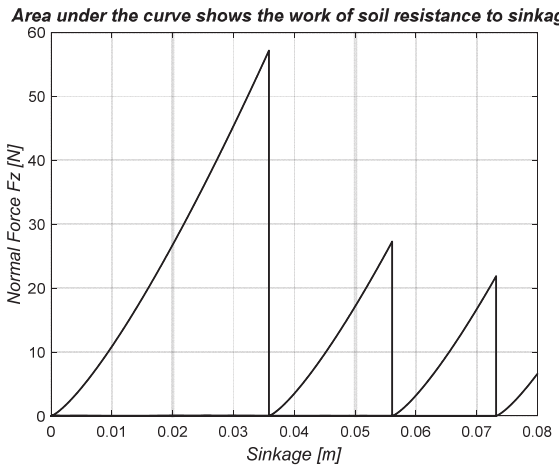

Fig. 14. The normal force which acts on the wheel during sinkage as function of the sinkage for constant soil parameters

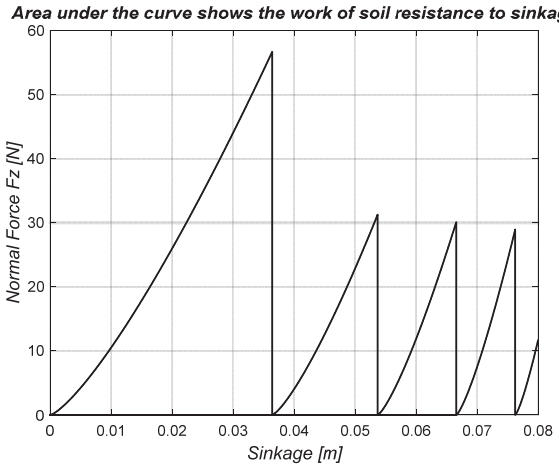

Fig. 15. The normal force which acts on the wheel during sinkage as function of the sinkage considering the soil's parameters change

mass displacement for comparison purpose. Point 1 in the figure represents the touch instant of the wheel with the soil. This is the start point of the system interaction. At this instant the initial values of motion of the two masses are the free fall velocities, zero initial displacement of the wheel, and body displacement equal to the unstretched length of the suspension spring. At point 2 wheel reaches its maximum sinkage and dwells for a very short period of time with zero velocity. Point 3 is the start of the wheel pull out of the soil until it reaches point 4.

5. Normal Force Work Estimation

The work *w* of the normal force during sinkage is determined by finding the area under the curves in Figures 14 & 15. A numerical integration is required to find the area for a nonlinear normal force curve. Fortunately the shape of the areas under the curve resembles a right angle triangular and can be approximated by finding the area of the triangle which one side of it is the maximum normal force at the maximum sinkage and the base is the maximum sinkage.

$$w = \frac{1}{2} F_z z_m = \frac{1}{2} k_z (z_m)^{n+\frac{3}{2}} \tag{32}$$

It can be noticed that the work of the normal force is a function of the maximum sinkage and the system--soil parameters Equation (32), and causes dissipation of the mechanical energy of the system.

6. Results and Discussion

The dynamic interaction between the rigid wheel (unsprung mass) and the soft soil for each fall has three stages. The three stages of the first fall are; first stage starts at point 1 and ends at point 2 as depicted in Figure 10, second stage starts at point 2 and ends at point 3, and the third stage starts at point 3 and ends at point 4. During the first stage, the wheel penetrates the soft soil until it reaches maximum sinkage with a maximum normal force. In the second stage the wheel dwells and the sprung mass continues to vibrate. At the third stage the wheel leaves the soil and the two masses vibrates together. During the last two stages the normal force is zero.

The interaction with the soft soil has a merit of "stiffness" and the soft soil behaves as a nonlinear spring as shown in Equation (24) which makes any fall "collision" softer, while the sinkage in the soil is deeper than a harder soil. A deeper sinkage decreases the ability of the wheel to pull out of the soil. In contrast, falling on a harder soil resulted in a smaller sinkage and increases the ability of the spring mass to pull out the wheel (unsprung mass). The behavior of the normal force coefficient k_z (soil stiffness) for a constant soil's parameters remains constant during all falls, and when the soil's parameters increase for any additional falls, the normal force coefficient k_z increases rapidly as shown in Figure 8. This increase is caused by the increase of soil compactness for each additional fall which leads to an increase in the soil weight density and cohesion. The increase in these soil properties increases the normal force coefficient.

The simulations were done for two cases, one case when the soil parameters were kept constant during the whole time period, while in the second case the soil cohesion and density are changed as a result of a multi fall of the wheel on the same spot of the soft soil. The multi fall case is considered as a multi passages wheel case and the previous proposed relations for a wheel multi passages were used.

The dynamic displacements of the wheel (unsprung mass), and the normal force during sinkage, for a multi fall of the wheel on the soft soil are shown for two cases. In the first case the soil's parameters were kept unchanged for all falls on the soil, Figures 10, and 12 respectively, while in the second case there was a change in the soil cohesion and soil density as a result of the wheel multi fall, Figures 11, and 13 respectively. Figures 14, and 15 show the normal force during sinkage as function of the sinkage for the two aforementioned cases respectively, where the areas under the curves give the work done by the normal forces.

By comparing the results of the simulation for the dynamic displacements, the normal forces, and the work of the normal forces in the two cases, it can be noticed that the changes in the first case are gradual changes along the whole period, while in the second

case the major changes occur between the first fall and the second fall, and monotonic changes occur between the second fall and the falls after in comparison to the second fall. This behavior is expected because the first fall makes the soil more compact, as a result the soil parameters are changed and the sinkage is much less than the first time and it is harder to penetrate into the soil, while during the successive falls by the same mass the soil's compactness increase is smaller resulting in smaller changes of the soil properties.

The normal force behavior during sinkage into the soft soil acts in a very short time and it has a geometric shape resemblance to an impulsive force during collision, therefore in future work the sinkage stage will be modeled as a collision of two bodies, a hard body and soft body.

The work of the normal force during sinkage dissipates the mechanical energy of the system. The dissipated energy in the first fall is the same in both cases. In the first case there is a gradual reduction of energy and in the second case the energy reduction in the successive falls is small. For a soil with a soil's exponent value n=0.5 the approximated work of the normal force has an energy expression as the work of a linear spring.

The simulation results show that by keeping the soil's parameters unchanged as a result of repetitive falls of a rotation less wheel, zero slip, has negligible effect on the dynamic behavior of the rover. For a rotation less wheel, zero slip, the second terms in both Equations (9) and (10) vanish. In this case there is no contribution of a sheer stress which leads to less compactness of the soil under the wheel. The existence of these terms in both equations add to the soil's density and soil's cohesion values up to 16.7% of the original values.

AUTHOR

Hassan Shibly – Central Connecticut State University New-Britain, CT, 06050, USA.
E-mail:hshibly@ccsu.edu.

REFERENCES

[1] E. Bernstien, *Probleme zur experimentellen motorplugmechanic*, Heft: Der Motorwagen 16, 1913.
[2] B. P. Goriatchkin, "T*heory and development of agriculture machinery*", 1938.
[3] M. G. Bekker, *Theory of land locomotion the mechanics of vehicle mobility*, University of Michigan Press, Ann Arbor, 1956.
[4] J. Wong, *Theory of ground vehicles*, New York: J. Wiley, 1993.
[5] J. Y. Wong, "On the study of wheel-soil interaction", *Journal of Terramechanics,* vol. 21, no. 2, 1984, 117–131. DOI: 10.1016/0022-4898(84)90017-X.
[6] S.K.Upadhyaya, D.Wulfsohn, J.Mehlschau, "An instrumented device to obtain traction related parameters", *Journal of Terramechanics,* vol. 30, 1993,1–20. DOI: 10.1016/0022-4898(93)90027-U.
[7] A. Reece, "Principles of soil vehicle mechanics". In: *Proceeding of the Institution of Mechanical Engineers*, 1965.
[8] G. Meirion-Griffith, M. Spenkom "A modified pressure-sinkage model for small rigid wheels on deformable terrains", *Journal of Terramechanics,* vol. 48, no. 2, 2011, 149–155. DOI: 10.1016/j.jterra.2011.01.001.
[9] J. Y. Wong, "An introduction to terramechanics", *Journal of Terramechanics,* vol. 21, no. 1, 1984, 5–17. DOI: 10.1016/0022-4898(84)90004-1.
[10] M. G. Bekker, *Off the Road Locomotion*, Ann Arbor, Michigan: The University of Michigan Press*,* 1960.
[11] M. G. Bekker, *Theory of Land Locomotion*, Ann Arbor, Michigan: The University of Michigan Press*,* 1965.
[12] A. Reece, "Problems of soil vehicle mechanics", ATAC, Warren, MI, USA, 1964.
[13] R. A. Liston, L. A. Martin, "Multipass behavior of a rigid wheel". In: *2 Proc. Sec. Int. Conf. on Terrain-Vehicle Systems*, Quebec City, Que., Toronto Univ. Press, 1966.
[14] I. C. Holm, "Multi-pass behaviour of pneumatic tires", *Journal of Terramechanics,* vol. 6, no.3, 1969, 347–71. DOI: 10.1016/0022-4898(69)90128-1.
[15] C. Senatore, C. Sandu, "Off-road tire modeling and the multi-pass effect for vehicle dynamics simulation", *Journal of Terramechanics,* vol. 48, no. 4, 2011, 265–276. DOI: 10.1016/j.jterra.2011.06.006.
[16] S. Shaaban, "Evolution of the bearing capacity of dry sand with its density", *Journal of Terramechanics,* vol. 20, nos. 3–4, 1983, 129–138. DOI: 10.1016/0022-4898(83)90044-7.
[17] D. Dewhirst, "A load-sinkage equation for lunar soil", *AIAA Journal,* vol. 2 (4)*,* 1963, 761–762.
[18] O. Onafeko, A.R. Reece, "Soil stresses and deformation beneath rigid wheels", *Journal of Terramechanics*", vol. 4, no. 1, 1967, 59–80. DOI: 10.1016/0022-4898(67)90104-8.
[19] I. Shmulevich, U. Mussel, D. Wolf, "The effect of velocity on rigid wheel Performance", *Journal of Terramechanics,* vol. 35, no. 3, 1998,189–207. DOI: 10.1016/S0022-4898(98)00022-6.
[20] M. Grahn, "Prediction of sinkage and rolling resistance for off the road vehicles considering penetration velocity", *Journal of Terramechanics,* vol. 28 , no. 4, 1991, 339–347. DOI: 0.1016/0022-4898(91)90015-X.
[21] H. Shibly, "Dynamic Modeling of Planetary Vehicle's Fall on Soft Soil", *Journal of Automation, Mobile Robotics, & Intelligent Systems,* vol. 10, no 3, 2016, 21–27. DOI: 10.14313/JAMRIS_3-2016/20.
[22] H. Shibly, K. Iagnemma, S. Dubowsky, "An equivalent soil mechanics formulation for rigid wheels in deformable terrain, with application to planetary exploration rovers", *Journal of Terramechanics,* vol. 42, no. 1, 2005, 1–13. DOI: 10.1016/j.jterra.2004.05.002.